Novel improved particle swarm optimization-extreme learning algorithm for state of charge estimation of lithium-ion batteries.

ZHANG, C., WANG, S., YU, C., XIE, Y. and FERNANDEZ, C.

2022

Novel Improved Particle Swarm Optimization-Extreme Learning Machine Algorithm for State of Charge Estimation of Lithium-Ion Batteries

Chuyan Zhang, Shunli Wang*, Chunmei Yu, Yanxin Xie, and Carlos Fernandez

Abstract

Incisively estimating the state of charge (SOC) of lithium-ion batteries is essential to ensure the safe and stable operation of a battery management system. Neural network methods do not depend on a specific lithium-ion battery model and are able to mirror the lithium-ion battery's nonlinear relationships, thus receiving widespread attention; however, traditional neural network methods exhibit a long training time and low accuracy in estimating SOC. This paper presents an original algorithm of an improved particle swarm optimization (IPSO) extreme learning machine (ELM) neural network, improving the particle swarm algorithm using nonlinear inertia weights to enhance the global optimization seeking capability of ELM for solving the problem of poor precision of previous battery SOC estimation. The lithium-ion battery voltage and current are the input variables of the model, while SOC is used as the output variable. The results of the experiments revealed that the root-mean-square estimation errors of the proposed IPSO-ELM algorithm for SOC are within 0.31, 0.32, and 0.14% of the root mean square under the hybrid pulse power characteristic (HPPC), the Beijing bus dynamic stress test (BBDST), and the dynamic stress test (DST) operating conditions. Compared with the prediction results of the PSO-ELM and ELM neural networks, the simulation results prove that the SOC optimization method in this paper possesses superior precision and overcomes the shortcomings of traditional neural networks.

1. Introduction

Energy security and the effectiveness of conserving the environment remain fundamental to China's expansion agenda. (1) Throughout all nations, renewable energy sources alternative to conventional fossil fuels are already in the spotlight. (2) The strengths of lithium-ion batteries with excellent density of energy, huge output capacity, and excellent cost–performance ratio have been broadly implemented and disseminated in the field of regenerative energy. (3) Its application permits the fabrication of functional electric vehicles and fulfills certain rigorous benchmarks of electric vehicle economics when it comes to energy density, endurance, safety, performance, and expense. (4) Nevertheless, the likelihood of battery pack flame (5) and ignition has not been not entirely eradicated. Consequently, an integrated and supported lithium-ion battery management system (6) acts as a key to the safety and optimal operation of lithium-ion batteries. Methodologies for battery modeling as well as state-of-charge estimation play an invaluable role in this field. (7) Provided that the model particles (8) are optimally defined, it turns out that the equivalent circuit models, which are both linear and nonlinear, (9) are found to be capable of forecasting the properties of all types of cells with various diameters, properties, capacities, and ingredients with appreciable precision. (10) According to the different mechanisms of battery modeling, the equivalent models of lithium-ion batteries can be classified into brief electrochemical models, (11) smart mathematical models, (12) and equivalent circuit models. (13) Considering that the variation of physical parameters (14) can reflect the internal degradation of a battery, instead, a simplified electrochemical model for which the

parameters are well recognizable is proposed, and the physical parameters of the cell can be obtained from its relation as a function of the parameter of the model. (15)

One of the most vital parameters describing the state of charge of a lithium-ion battery's residual capacity is its lifetime. (16) The charging state of lithium-ion batteries is impacted by their internal electrochemical reactions, charging and discharging mechanisms, as well as outside environmental circumstances, in terms of charge/discharge ratios, self-discharge, temperature, and extent of aging. (17) Currently, approaches toward assessing lithium-ion batteries' state of charge involve (18−23) the open-circuit voltage approach, the ampere–time integral approach, the discharge approach, the data-driven approach, the Kalman filter approach, and the particle filter approach. The approach to on-voltage is designed to evaluate state of charge (SOC) by exploiting the nearly linear dependence that exists regarding SOC and on-voltage. (24) The ampere–time integrated method is applied to evaluate the state of charge of a battery as it accumulates the amount of charging and discharging that occurs while charging and discharging a battery. (25) The Kalman filter approach is one of the best digital manipulation algorithms, and its derivatives include (26) the extended Kalman filter, the traceless Kalman filter, the adaptive Kalman filter, and the particle filter. The exact accuracy of the Kalman filtering approach (27) lies in an appropriate and valid model of the cells, but accurate cell models are difficult to obtain. Data-driven methods (28) are approaches for estimating SOC building on machine learning policies, which include methods of neural network (NN), (29) deep learning (DL) method, (30) support vector machine, (31) and fuzzy logic method. (32) Of all these, it is the neural network method that is the widest in use. With this method, no knowledge of the internal construction of a battery is required (33) and one can modify the battery immediately on the basis of a large quantity of training data.

Extreme learning machine is a fast single-stack implicit feed-forward neural network, (34) and it is advantageous when compared to classical feed-forward neural networks. (35) The extreme learning machine (ELM) approach yields the joint weights of the input and hidden layers stochastically, which suffers from poor training speed, prone to drop into certain areas of local minimax, and sensitive choice of studying ratio. (36) No adjustment of the threshold value of the implicit-layer neurons is needed when training, and one can merely tune the number of implicit-layer neurons to yield the exclusive optimal outcome. (37) In contrast to classical training approaches, the ELM approach possesses quick learning speed and brilliant generalization characteristic. (38)

In addition, the ELM network characteristics also make the prediction results occasionally deviate significantly in the prediction process. The cause is the stochastic generation of parameters at the entry side of the network leading to complex covariance with a certain probability, which in turn frequently leads to random volatility of the network output, so that the robustness of its forecasting results is decreased. In this paper, it is recommended that the input side of the extreme learning machine be refined using the superior worldwide search engine capability of the improved particle swarm algorithm and also decrease the complexity of the model training. The objective is to further enhance the stability of the prediction results while guaranteeing the SOC prediction precision of the model, thus ensuring the credibility of the prediction results.

2. Theoretical Analysis

2.1. Extreme Learning Machine

The extreme learning machine is employed to forecast the outputs of sophisticated nonlinear systems. (39) It has advantages such as a lower training factor, quicker acquisition, and stronger proficiency in generalization. A three-layer configuration consisting of an import layer, an implicit layer, and an

export layer is adopted by the extreme learning machine, which acts on a stochastic foundation. (40) The joint weights are generated stochastically in the operation from the import layer to the implicit layer, as well as the thresholds of those neurons in the implicit layer. (41) With the structure illustrated in Figure 1, the process goes as follows.

Figure 1

Figure 1. ELM network structure.

It is assumed that there are N diverse sets of samples for training

$$E = \{(x_p, y_p) | p = 1, 2, \cdots, N, x_p \in R^n, y_p \in R^m\} \quad (1)$$

In eq 1, $x_p \in R^n$, indicating the size of the n-dimensional input variable; and $y_p \in R^m$, indicating the adequate destination vector for export. If there exist k quantities of neurons in the ELM implicit layer, then when the input specification becomes xp, the relevant true output of the ELM can be denoted as

$$y_p = \sum_{j=1}^{k} \beta_j g(\omega_j, x_p, b_j), p = 1, 2, \cdots, N \quad (2)$$

In eq 2, ω_j denotes the joint weights of the sheltered layer neurons in relation to each unit in the introductory layer, b_j (j = 1,2,⋯,*L)* indicates the threshold value of the *i*-th implicit-layer interneuron, g() indicates activated by the function, and β_j indicates the joint weights of the implicit-layer neurons that correspond to the units in the export layer.

Equation 2 is then simplified to derive

$$H\beta = Y' \quad (3)$$

In eq 3, Y' is the output matrix, β is the matrix of export values of the weights, and H is the export matrix of the implicit layer, denoted by eq 4

$$H = \begin{bmatrix} g(\omega_1 x_1 + b_1) & g(\omega_2 x_1 + b_2) & \cdots & g(\omega_L x_1 + b_L) \\ g(\omega_1 x_2 + b_1) & g(\omega_2 x_2 + b_2) & \cdots & g(\omega_L x_2 + b_L) \\ \vdots & \vdots & \ddots & \vdots \\ g(\omega_1 x_K + b_1) & g(\omega_2 x_N + b_2) & \cdots & g(\omega_L x_N + b_L) \end{bmatrix} \quad (4)$$

$$\beta = [\beta_1, \beta_2, \cdots, \beta_L]^T \quad (5)$$

$$Y' = [y_1, y_2, \cdots, y_N]^T \quad (6)$$

With the definition of the Moore–Penrose broad inverse matrix, (42) it can be concluded that

$$\beta = H^{+}Y' \tag{7}$$

There is a generalized reciprocal matrix H of H^{+} in eq 7.

2.2. Improved Particle Swarm Optimization Algorithm

The particle swarm optimization (PSO) algorithm is a calculative technique that is used for evolution. (43) Based on the study of bird feeding performance, the underlying ideas of PSO comprise searching for the optimal method by sharing data among individuals. The individual birds are the particles used in the PSO algorithm. (44) As an efficient parallel optimization algorithm, PSO tackles a vast number of nonlinear, nondifferentiable, and multipeaked complex issues. It has developed dramatically due to its straightforward implementation and the small number of parameters to be tuned. Different types of improved particle swarm optimization algorithms have emerged and have been successfully applied in many scientific and engineering areas. In this paper, nonlinear inertia weights are used to improve the particle swarm algorithm based on the powerful optimization capability of the particle swarm algorithm and its series of excellent performances in neural network weight optimization, based on the study of inertia weights of critical parameters of the particle swarm algorithm. (45)

For the particle *i*, its position in N-dimensional space is denoted with the vector $x_i = (x_{i1}, x_{i2},\cdots,x_{ip})$ and the rate of flight is denoted with the vector $v_i = (v_{i1},v_{i2},\cdots,v_{ip})$. There is a utility value for each particle, it is drawn by the goal function as well as knows the optimal location which it found so far (p_b) and the location xi where it is right now. Additionally, which can be viewed as the experienced flight owned by the particle itself. In addition, each particle knows the optimal location (pg) of the whole set of particles detected up to now. That is precisely what particles do when they utilize their own experience as well as the optimal experience of their peers to decide their future actions. (46)

It is initially generated by the PSO as a cluster of stochastic particles. (47) Then, the optimal useable settlement is found through iterations. The particles upgrade themselves in each iteration by tracking the two "extremes" (p_b, p_g). (48) When the two optimal values are identified, then the particle updates its rate and position by applying eqs 8 and 9.

$$x_{iq}^{\,m+1} = \omega v_{iq}^{\,m} + x_1\varepsilon(p_{iq}^{\,m} - x_{iq}^{\,m}) + x_2\varepsilon(p_{gq}^{\,m} - x_{iq}^{\,m}) \tag{8}$$

$$x_{iq}^{\,m+1} = x_{iq}^{\,m} + v_{iq}^{\,m} \tag{9}$$

In the equation, ω is the inertial constant, viq is the velocity q-dimensional component of particle i at the m-th iteration, x_{iq} denotes the position q-dimensional component of particle i at the m-th iteration, p_{iq} denotes the q-dimensional component of particle i at the best position, p_{gq} denotes the q-dimensional component of the best position of all particles, x_1 and x_2 are weight factors, and ε is a stochastic number between [0, 1]. Based on this, this research proposes to replace the fixed weight with a variable ω, as shown in eq 10.

$$\omega_o = \omega_{end} + (\omega_{start} - \omega_{end}) \times \left(1 - \frac{t}{t_{max}}\right) \tag{10}$$

In eq 10, t_{max} is the maximal number of iterations allowed and ωs_{tart} and ω_{end} are the original set of inertia weights and the values as it expands to the largest permissible amount of iterations. Through

several experiments, it is found that the implementation of the IPSO algorithm will have a dramatically enhanced performance when $\omega_{start} = 0.8$ and $\omega_{end} = 0.3$, as the linear weight reduction strategy is straightforward and intuitive, which has superior optimization performance. Nevertheless, the search process of particle swarm is nonlinear and sophisticated. During the sophisticated ω generation process, the linear transformation fails to accurately capture the search process. The particle swarm is supposed to have a large ω value at the initiation of the iteration and a small ω value at the termination of the iteration. Based on this, this investigation improves the decreasing strategy shown in eq 11.

$$\omega_o = \omega_{end} + (\omega_{start} - \omega_{end}) \times \left[1 - \left(\frac{t}{t_{max}}\right)^{1/1+e^{-2x}}\right]^{1/1+e^{-x}} \quad (11)$$

The process of the IPSO algorithm is presented in Figure 2.

(1) A group of particles (the group size is N) is initialized, composed of random positions as well as rates.

(2) The adaptability value of each particle is assessed.

(3) A comparison is drawn for each particle between the fitness value and the best fitness p_b it passes through, and if it is larger, then it is adopted as the current individual extreme p_b. Similarly, the global extreme p_g is updated.

(4) The weights ω are updated on the basis of eq 11.

(5) The rate and position of the particles are adapted in accordance with eqs 8 and 9.

(6) If the maximum number of iterations or the best adaptability is not satisfied, go to (step 2).

(7) End.

Figure 2

Figure 2. Flowchart of the standard IPSO algorithm.

2.3. IPSO-ELM Algorithm

The stochastic character of the ELM priming leads to various issues that inherently arise in the model, which decreases the prediction precision. (49) Therefore, in this section, the IPSO algorithm is adopted to search for the best parameters of ELM, while the IPSO-ELM model (50) is built to improve the low prediction accuracy of SOC. Figure 3 illustrates the flowchart of the IPSO-ELM algorithm, which is in accordance with the evaluation of the SOC of lithium-ion batteries.

Figure 3

Figure 3. Flowchart of the SOC estimation based on IPSO-ELM.

The detailed steps are listed as follows.

(1) The particle population is initialized, as well as the stochastically generated input weights and thresholds are fed into the ELM training algorithm.

(2)

The fitness evaluation is performed for each particle, and the root-mean-square error of the training set is taken as the fitness function of the particle

$$f_{\mathrm{RMSE}} = \sqrt{\frac{\sum_{\mathrm{p}=1}^{N} \| \sum_{j=1}^{K} \beta_j g(\omega_j, x_{\mathrm{p}}, b_j) - t_{\mathrm{p}} \|_2^2}{N}} \tag{12}$$

In eq 12, N is the sample number.

(3) Update local optimal particles and global optimal particles.

(4) Update the location and rate of particles to acquire new particles during the iteration.

(5) Identify if the ending condition is fulfilled (maximum number of iterations reached). Quit to recover the optimal individual if it is satisfied; otherwise, jump to (step 2) and continue.

3. Experimental Analysis

3.1. Simulation Results and Analysis under the HPPC Condition

For this experiment, a lithium-ion battery whose rated capacity is 4.2 V/50 Ah has been chosen as the experimental object. The experimental battery hybrid pulse power characteristic (HPPC) charging and discharging equipment is the model BTS200-100-104 power battery high-rate charging and discharging instrument for power batteries manufactured by Shenzhen Xinwei New Energy Technology Co. The apparatus is a triply temperature-independent high- and low-temperature chamber that operates at a controlled temperature of 25 °C from Dongguan Bell Experimental Equipment Co. The pulse characteristic curve of the cell is shown in Figure 4.

Figure 4

Figure 4. HPPC experimental voltage and current curve.

To prove that the model presented in this paper has a stronger performance, IPSO-ELM (the method proposed in this research) and PSO-ELM (the traditional particle swarm optimization-extreme learning machine method) were established. A comparison of the optimization results in this paper is plotted for a more intuitive observation, as shown in Figure 5.

Figure 5

Figure 5. Optimal adaptability curves.

Figure 5 illustrates that PSO falls into the local optimal solution at about 180 iterations. Nevertheless, IPSO remains optimized at 400 iterations when the optimal result is about 73%. Comparing the optimal results of IPSO with those of PSO, the difference between the optimal results of IPSO and PSO is about 10%, which verifies the apparently enhanced optimization capability of IPSO. After training the model using the sample data set, test samples of the network are selected to test the trained IPSO-ELM model. The first 70% of the sample data were chosen as the training data, through which the model was trained, and then, the complete data with SOC of 0–1 were selected as the test data for the error analysis. A comparison of the prediction results of the IPSO-ELM algorithm proposed in this paper with the PSO-ELM algorithm and the ELM algorithm is carried out empirically, and the results are shown in Figure 6.

Figure 6

Figure 6. Comparison of SOC estimation results under the HPPC condition.

It is clear from Figures 6 and 7 that the tendency of the predicted SOC values based on IPSO-ELM is quite similar to the actual SOC values of the lithium-ion battery, thus proving the validity of the proposed model. In addition, the predicted values of the improved IPSO-ELM are more accurate than those of the unmodified PSO-ELM, and the absolute errors of the estimates are all under 1%, which fully meets the demands of SOC estimation for lithium-ion batteries. The IPSO-ELM method proposed in this paper has performed relatively well in terms of estimation precision and stability, which also demonstrates that the lithium-ion battery SOC estimation algorithm based on the optimized ELM of the IPSO algorithm proposed in this paper works effectively and feasibly.

Figure 7

Figure 7. Error curves of SOC estimation under the HPPC condition.

Both the mean absolute error (MAE) and the root-mean-square error (RMSE) are brought in for evaluation to better assess the prediction performance of respective models. The smaller the MAE value, the better the quality of the model and the better the accuracy of the prediction. The smaller the value of RMSE, the better the generalization performance of the prediction model. Meanwhile, the MAE and RMSE are expressed as follows

$$\mathrm{MAE} = \frac{1}{N}\sum_{i=1}^{N}|\mathrm{X}_i - \hat{\mathrm{X}}_i| \tag{13}$$

$$\mathrm{RMSE} = \sqrt{\frac{1}{N}\left(\sum_{i=1}^{N}(\mathrm{X}_i - \hat{\mathrm{X}}_i)^2\right)} \tag{14}$$

Furthermore, it is clearly seen from Table 1 that the RMSE and MAE of the refined IPSO-ELM model are 0.31 and 0.26%, respectively, compared with the unmodified PSO-ELM and ELM models. It is further demonstrated that the refined IPSO-ELM model has excellent estimation precision, offers a better fit, and its prediction speed is rapid.

Table 1. SOC Estimation Error Results under the HPPC Condition

algorithm	MAE (%)	RMSE (%)	running time (s)
ELM	2.02	2.37	31.23
PSO-ELM	1.92	2.27	55.91
IPSO-ELM	0.26	0.31	53.21

3.2. Simulation Results and Analysis under the BBDST Condition

The lithium battery employed is the LFP50AH ternary lithium battery, which is tested with reference to the operating conditions set by the BBDST. The experimental battery charging and discharging equipment BTS750-200-100-4 Battery Test Device was supplied by Shenzhen Yakeyuan Technology Co.

Figure 8a,b illustrates data on experimental currents and voltages under the operating conditions of the BBDST. As the BBDST conditions of operation are power discharges, it is observed that as the loop count rises, the discharge current grows and the battery end voltage overall shows a declining trend.

Figure 8

Figure 8. BBDST experimental voltage and current curve.

The top 70% of the data were chosen for model training from the data sets that were used for the experiments under the BBDST condition, and then, the complete data with SOC of 0–1 were selected as the test samples of the network to test the trained model. The prediction results of the ELM model and the PSO-ELM model were compared with the IPSO-ELM model proposed in this paper, and the results of the experiment are displayed in Figure 9.

Figure 9

Figure 9. Comparison of SOC estimation results under BBDST condition.

The SOC estimation results of different algorithms on the test set under the BBDST condition are presented in Figure 9, and the estimation errors are presented in Figure 10. It can be seen from Figures 9 and 10 that the ELM and PSO-ELM estimation results do not converge properly to the true value, especially in the late stage of estimation, which shows a divergence trend and poor stability, and the estimation errors of the two algorithms reach 8 and 3%, respectively, which cannot fulfill the actual needs. The refined IPSO-ELM model has favorable convergence, and its estimation error is reduced to within 1% apart from individual points, which have a higher estimation precision. The IPSO algorithm offers a greater global discovery capability than the PSO algorithm, which enables IPSO-ELM to obtain the optimal model parameters, and the estimated model thus obtains better generalization performance.

Figure 10

Figure 10. Error curves of SOC estimation under the BBDST condition.

The evaluation results of the estimation errors of the three algorithms on the test set are shown in Table 2. It can be evidently seen that the error values of IPSO-ELM are outperformed by the PSO-ELM and ELM algorithms for both RMSE and MAE. The foregoing shows that optimizing ELM parameters with the IPSO algorithm effectively enhances the generalization ability of the ELM model, and SOC estimation can be performed with more accurate prediction accuracy and a shorter running time.

Table 2. SOC Estimation Error Results under the BBDST Condition

algorithm	MAE (%)	RMSE (%)	running time (s)
ELM	0.46	0.68	21.52
PSO-ELM	0.23	0.34	61.73
IPSO-ELM	0.20	0.32	55.64

3.3. Simulation Results and Analysis under the DST Condition

DST represents a complex working condition with simplified urban operation conditions in the United States. With the purpose of further testing the SOC estimation accuracy of the IPSO-ELM algorithm, the DST working condition test was conducted for a ternary lithium battery with a rated capacity of 70AH at 25 °C, and the BTS200-100-104 battery test equipment provided by Shenzhen Yakeyuan Technology Co., Ltd. was selected as the experimental platform. The voltage and current curves are shown in Figure 11.

Figure 11

Figure 11. DST experimental voltage and current curve.

Under the condition of DST, the first 70% of the experimental data set was used to select as the model training, and then, the full data with SOC of 0–1 were selected as the test sample of the network to test the learned model. The prediction results of the ELM model and the PSO-ELM model were compared with the IPSO-ELM model proposed in this paper, and the experimental results are shown in Figure 12.

Figure 12

Figure 12. Comparison of SOC estimation results under the DST condition.

It is evident from Figures 12 and 13 that the estimation error of the ELM model is larger than 4% at the final stage, and the precision of estimation is not good. The IPSO-ELM algorithm with parameter optimization has superior convergence and stability to the PSO-ELM and ELM, and its estimated value

fluctuates slightly around the true value, and the absolute error of the test set is less than 1%, which perfectly suits the demand for SOC estimation for lithium-ion batteries.

Figure 13

Figure 13. Error curves of SOC estimation under the DST condition.

For more visual analysis of the prediction results of each model, the prediction results are statistically presented as shown in Table 3.

Table 3. SOC Estimation Error Results under the DST Condition

algorithm	MAE (%)	RMSE (%)	running time (s)
ELM	0.40	0.78	60.78
PSO-ELM	0.29	0.36	72.17
IPSO-ELM	0.11	0.14	68.34

As can be observed from Table 3, the refined IPSO-ELM algorithm has better RMSE and MAE than PSO-ELM and ELM. The SOC estimation error of the refined IPSO-ELM algorithm drops further compared to the PSO-ELM algorithm, with MAE and RMSE dropping to 0.11 and 0.14%, respectively. It shows that the suggested model is better than the PSO-ELM and ELM in performing lithium-ion battery SOC prediction; the optimization of the initial population by the IPSO algorithm enhances the ability of the algorithm to seek the optimal performance and is able to obtain a more precise model parameter in ELM.

4. Conclusions

For the characteristics of energy storage lithium-ion batteries with strong nonlinearity, within this paper, an IPSO-ELM neural network algorithm to enhance the performance of SOC estimation is proposed. The IPSO-ELM method is extremely valuable when the input data (currents and voltages) are used for SOC estimation. Under the operating conditions of HPPC, BBDST, and DST, the IPSO-ELM model proposed in this paper generates lower MAE and RMSE compared to ELM methods. A comparison with the PSO-ELM model shows that IPSO-ELM generates lower test MAE and a sensible training time, and none of the test RMSE of IPSO-ELM exceeded 0.5%; it also improved the global optimization seeking capability of ELM and obtained more accurate model parameters. Therefore, the SOC values of lithium-ion batteries derived from IPSO-ELM can adequately reflect the latest trends in lithium-ion battery charge states. The outcomes show the high estimation accuracy and robustness of the IPSO-ELM algorithm for estimating the SOC of lithium-ion batteries. The subsequent further plan of the proposed IPSO-ELM model is supposed to enhance the computational efficiency and decrease the time expenditure while ensuring prediction accuracy. Further, the proposed algorithm is combined with deep learning to optimize and increase prediction efficiency.

Author Information

Corresponding Author

Shunli Wang - College of Electrical Engineering, Sichuan University, Chengdu610065, China; School of Information Engineering, Southwest University of Science and Technology, Mianyang621010, China; Orcidhttps://orcid.org/0000-0003-0485-8082; Email: 497420789@qq.com

Authors

Chuyan Zhang - School of Information Engineering, Southwest University of Science and Technology, Mianyang621010, China; Orcidhttps://orcid.org/0000-0001-9200-0734

Chunmei Yu - College of Electrical Engineering, Sichuan University, Chengdu610065, China; School of Information Engineering, Southwest University of Science and Technology, Mianyang621010, China

Yanxin Xie - School of Information Engineering, Southwest University of Science and Technology, Mianyang621010, China

Carlos Fernandez - School of Pharmacy and Life Sciences, Robert Gordon University, AberdeenAB10 7GJ, U.K.

Notes

The authors declare no competing financial interest.

Acknowledgments

This work was supported by the National Natural Science Foundation of China (Nos. 62173281 and 61801407).

Figures

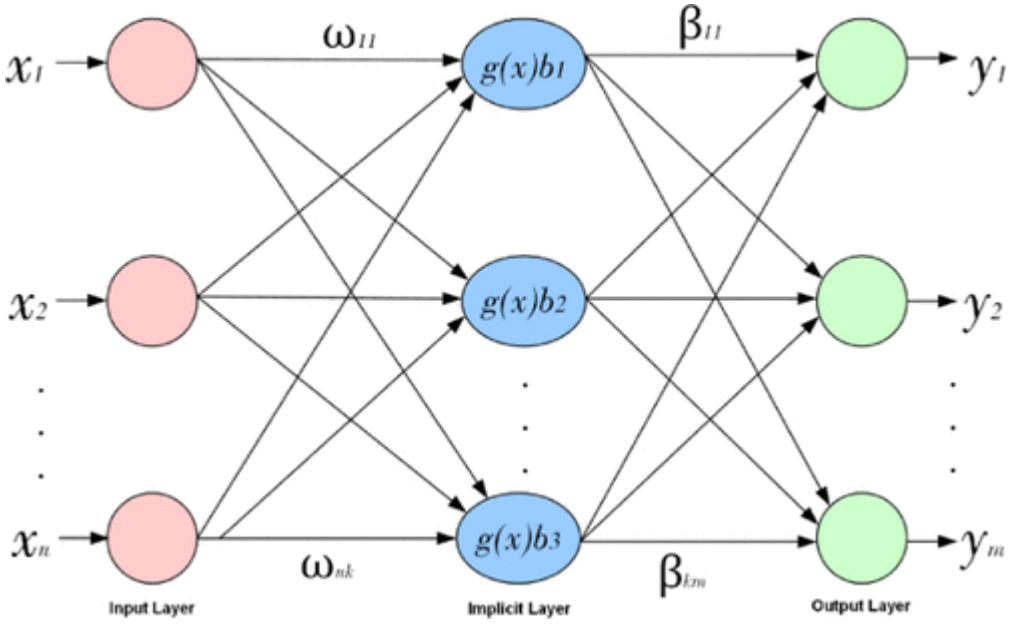

Figure 1. ELM network structure.

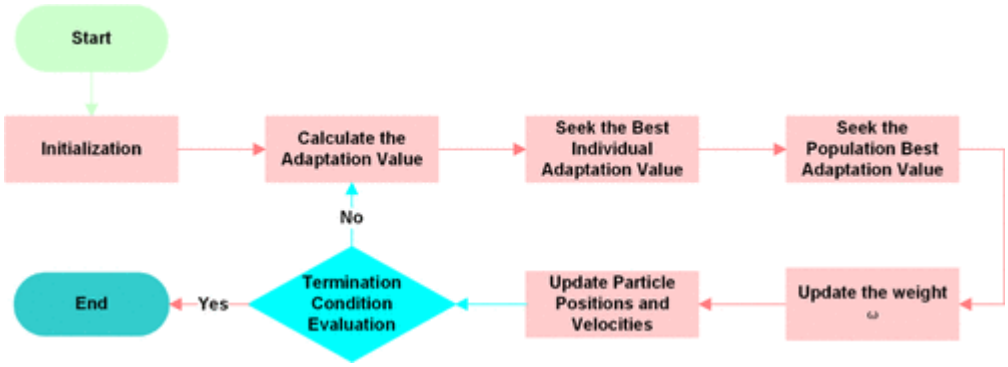

Figure 2. Flowchart of the standard IPSO algorithm

Figure 3. Flowchart of the SOC estimation based on IPSO-ELM.

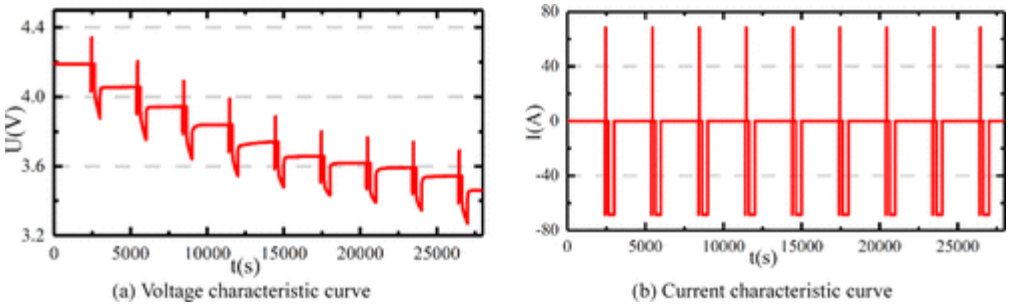

(a) Voltage characteristic curve (b) Current characteristic curve

Figure 4. HPPC experimental voltage and current curve.

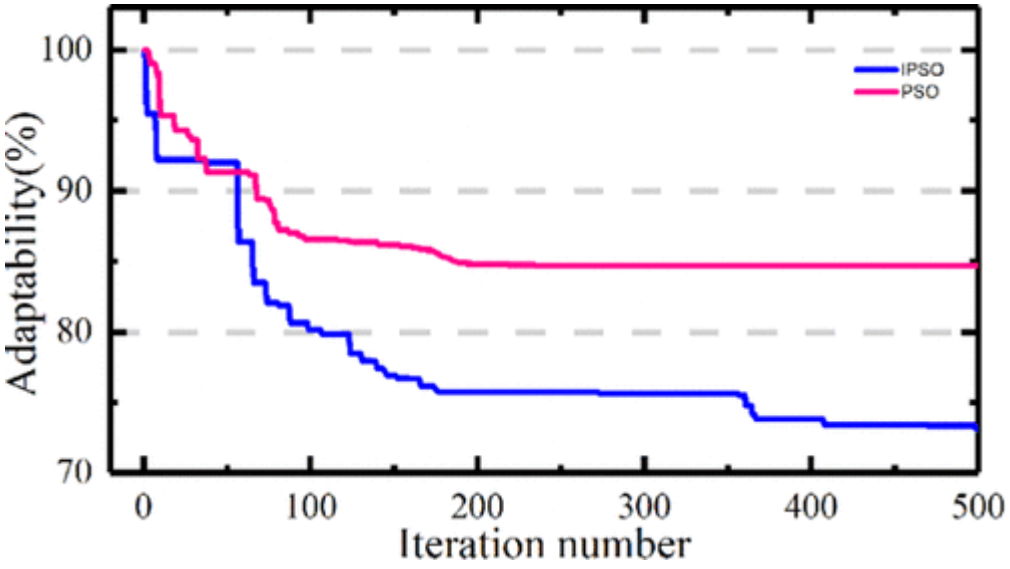

Figure 5. Optimal adaptability curves.

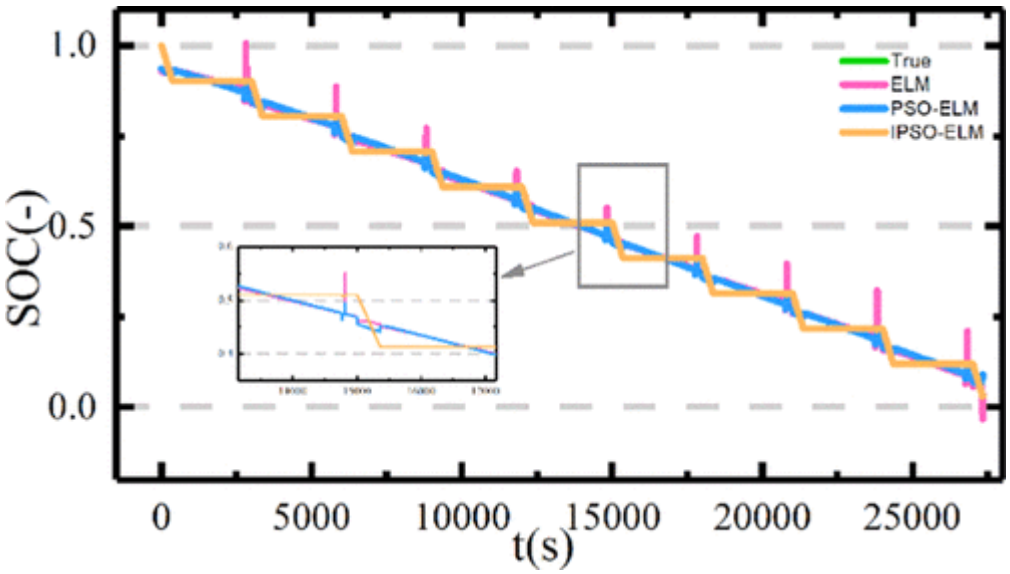

Figure 6. Comparison of SOC estimation results under the HPPC condition.

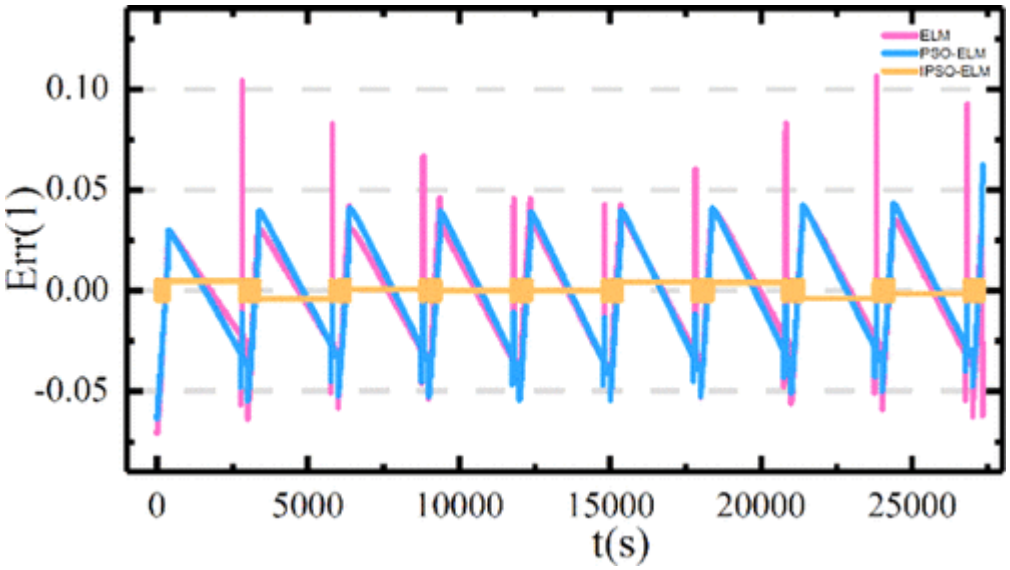

Figure 7. Error curves of SOC estimation under the HPPC condition

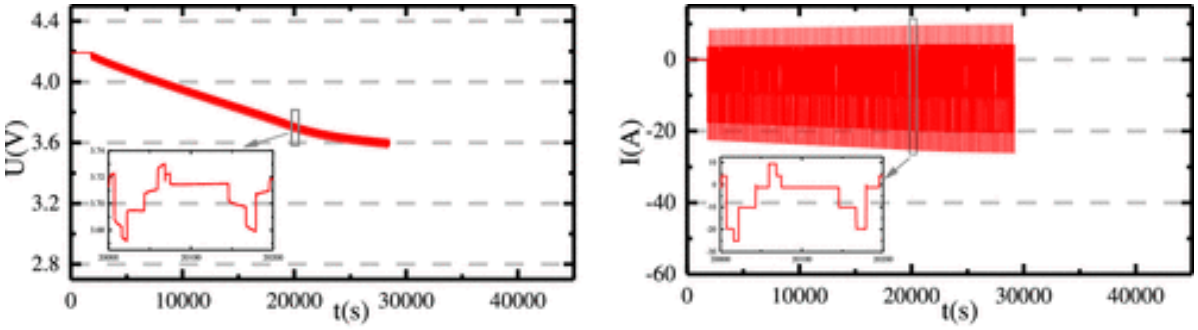

(a) Voltage characteristic curve

(b) Current characteristic curve

Figure 8. BBDST experimental voltage and current curve.

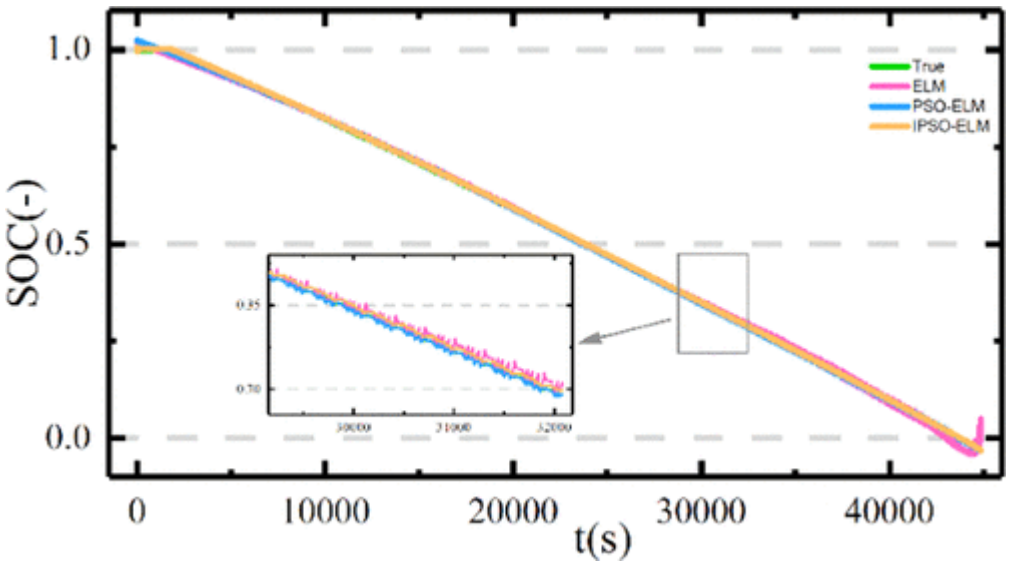

Figure 9. Comparison of SOC estimation results under BBDST condition

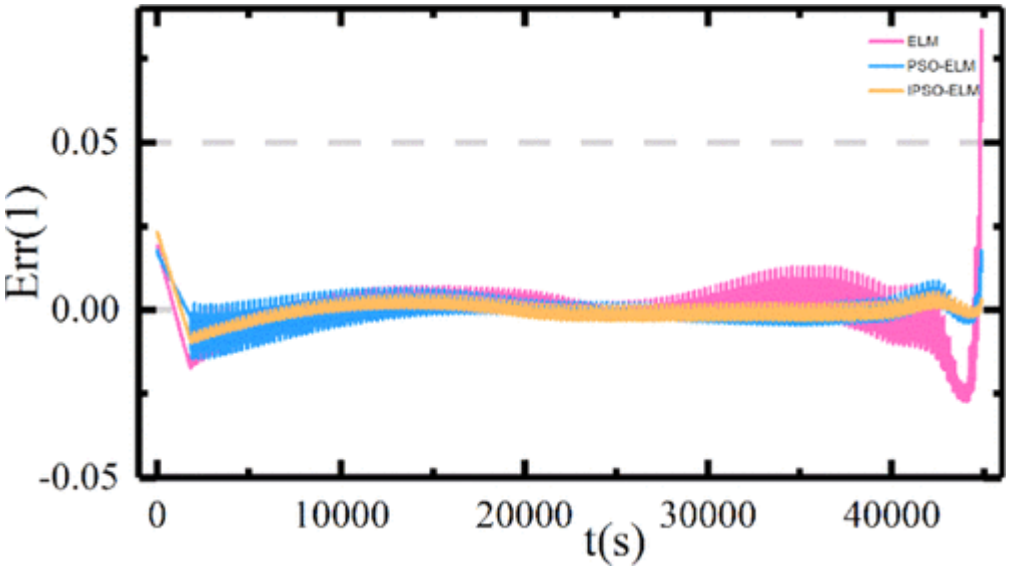

Figure 10. Error curves of SOC estimation under the BBDST condition.

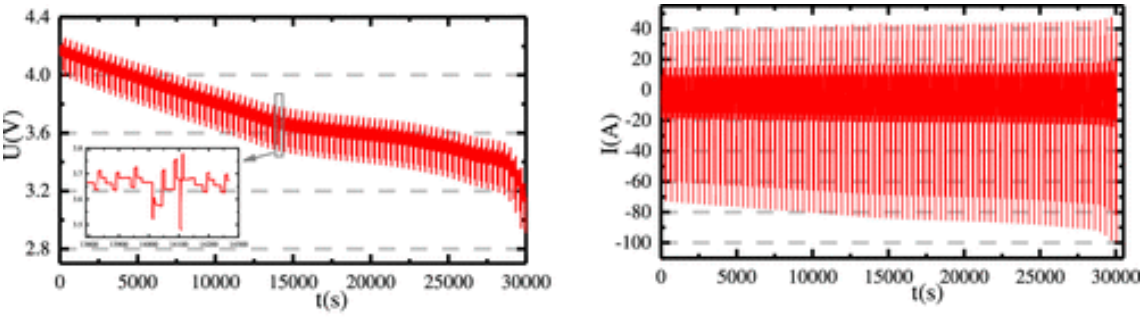

(a) Voltage characteristic curve

(b) Current characteristic curve

Figure 11. DST experimental voltage and current curve.

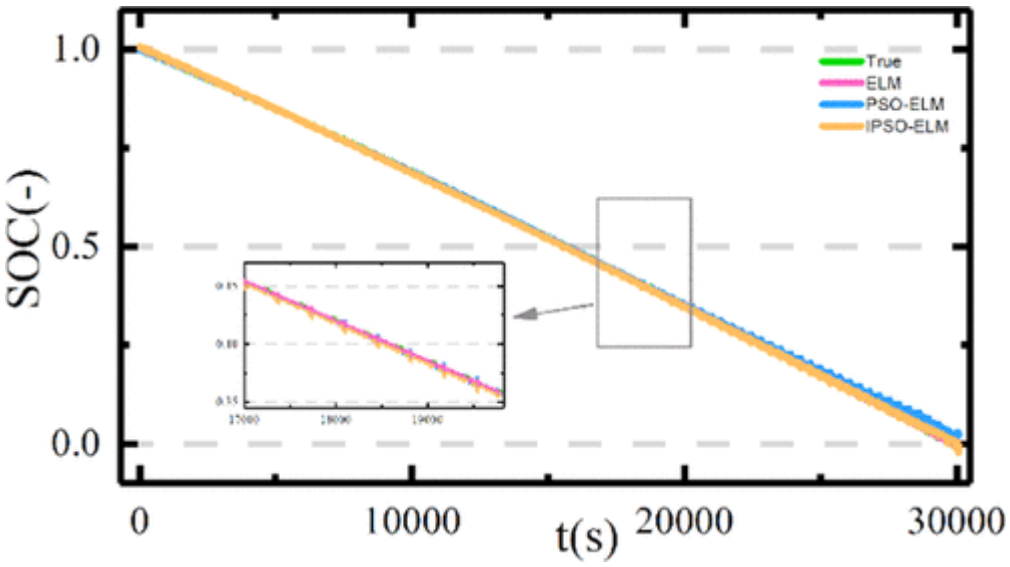

Figure 12. Comparison of SOC estimation results under the DST condition.

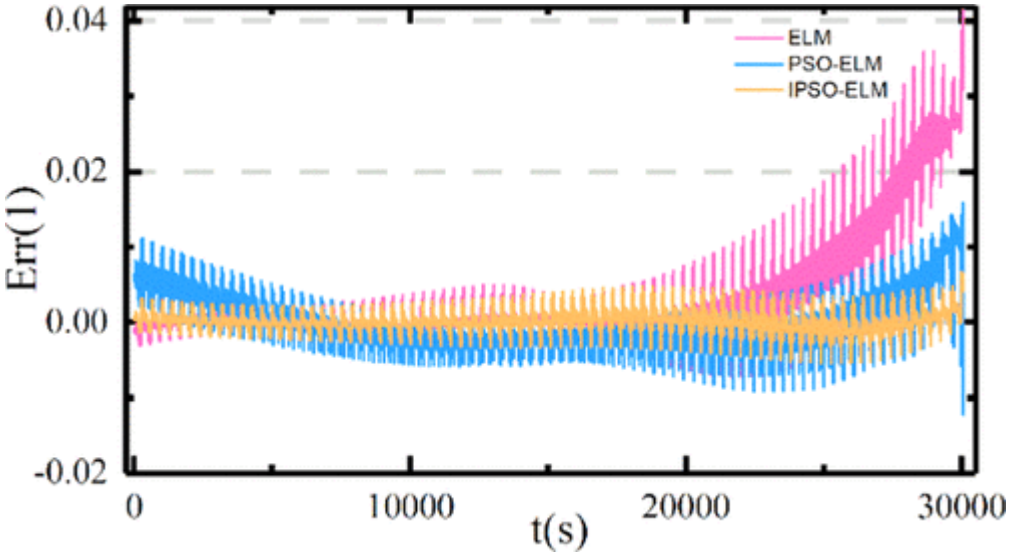

Figure 13. Error curves of SOC estimation under the DST condition

References

1Liu, P. K.; Hei, Z. H. Strategic Analysis and Framework Design on International Cooperation for Energy Transition: A perspective from China. Energy Rep. 2022, 8, 2601– 2616, DOI: 10.1016/j.egyr.2022.01.173 [Crossref], Google Scholar

2Xiong, H. Y.; Liu, H.; Zhang, R. H.; Yu, L. M.; Zong, Z. J.; Zhang, M. H.; Li, Z. An Energy Matching Method for Battery Electric Vehicle and Hydrogen Fuel Cell Vehicle Based on Source Energy Consumption Rate. Int. J. Hydrogen Energy 2019, 44, 29733– 29742, DOI: 10.1016/j.ijhydene.2019.02.169 [Crossref], [CAS], Google Scholar

3Zhang, X.; Han, Y.; Zhang, W. P. A Review of Factors Affecting the Lifespan of Lithium-ion Battery and its Health Estimation Methods. Trans. Electr. Electron. Mater. 2021, 22, 567– 574, DOI: 10.1007/s42341-021-00357-6 [Crossref], Google Scholar

4Geronikolos, I.; Potoglou, D. An Exploration of Electric-Car Mobility in Greece: A Stakeholders' Perspective. Case Stud. Transp. Policy 2021, 9, 906– 912, DOI: 10.1016/j.cstp.2021.04.010 [Crossref], Google Scholar

5Sripad, S.; Bills, A.; Viswanathan, V. A Review of Safety Considerations for Batteries in Aircraft with Electric Propulsion. MRS Bull. 2021, 46, 435– 442, DOI: 10.1557/s43577-021-00097-1 [Crossref], [CAS], Google Scholar

6Liu, Y. F.; Li, J. Q.; Zhang, G.; Hua, B.; Xiong, N. State of Charge Estimation of Lithium-Ion Batteries Based on Temporal Convolutional Network and Transfer Learning. IEEE Access 2021, 9, 34177– 34187, DOI: 10.1109/ACCESS.2021.3057371 [Crossref], Google Scholar

7Fotouhi, A.; Auger, D. J.; Propp, K.; Longo, S.; Wild, M. A Review on Electric Vehicle Battery Modelling: From Lithium-Ion toward Lithium-Sulphur. Renewable Sustainable Energy Rev. 2016, 56, 1008– 1021, DOI: 10.1016/j.rser.2015.12.009 [Crossref], [CAS], Google Scholar

8Guo, F.; Hu, G. D.; Zhou, P. K.; Huang, T. X.; Chen, X.; Ye, M. Q.; He, J. J. The Equivalent Circuit Battery Model Parameter Sensitivity Analysis for Lithium-Ion Batteries by Monte Carlo Simulation. Int. J. Energy Res. 2019, 43, 9013– 9024, DOI: 10.1002/er.4863 [Crossref], [CAS], Google Scholar

9Shaheen, A. M.; Hamida, M. A.; El-Sehiemy, R. A.; Elattar, E. E. Optimal Parameter Identification of Linear and Non-Linear Models for Li-Ion Battery Cells. Energy Rep. 2021, 7, 7170– 7185, DOI: 10.1016/j.egyr.2021.10.086 [Crossref], Google Scholar

10Malik, A.; Zhang, Z. M.; Agarwal, R. K. Extraction of Battery Parameters Using a Multi-Objective Genetic Algorithm with a Non-Linear Circuit Model. J. Power Sources 2014, 259, 76– 86, DOI: 10.1016/j.jpowsour.2014.02.062 [Crossref], [CAS], Google Scholar

11Verma, M. K. S.; Basu, S.; Patil, R. S.; Hariharan, K. S.; Adiga, S. P.; Kolake, S. M.; Oh, D.; Song, T.; Sung, Y. On-Board State Estimation in Electrical Vehicles: Achieving Accuracy and Computational Efficiency Through an Electrochemical Model. IEEE Trans. Veh. Technol. 2020, 69, 2563– 2575, DOI: 10.1109/TVT.2020.2966266 [Crossref], Google Scholar

12Ren, L.; Dong, J. B.; Wang, X. K.; Meng, Z. H.; Zhao, L.; Deen, M. J. A Data-Driven Auto-CNN-LSTM Prediction Model for Lithium-Ion Battery Remaining Useful Life. IEEE Trans. Ind. Inf. 2021, 17, 3478– 3487, DOI: 10.1109/TII.2020.3008223 [Crossref], Google Scholar

13Su, J.; Lin, M.; Wang, S. L.; Li, J.; Coffie-Ken, J.; Xie, F. An Equivalent Circuit Model Analysis for the Lithium-Ion Battery Pack in Pure Electric Vehicles. Meas. Control 2019, 52, 193– 201, DOI: 10.1177/0020294019827338 [Crossref], Google Scholar

14Han, X.; Feng, X.; Ouyang, M.; Lu, L.; Li, J.; Zheng, Y.; Li, Z. A Comparative Study of Charging Voltage Curve Analysis and State of Health Estimation of Lithium-ion Batteries in Electric Vehicle. Automot. Innovation 2019, 2, 263– 275, DOI: 10.1007/s42154-019-00080-2 [Crossref], Google Scholar

15Li, X. W.; Zhao, F.; Hou, J. L.; Guo, W. Features and Spread Mechanism of Thermal Runaway for Electric Car Batteries. Int. J. Heat Technol. 2021, 39, 1066– 1074, DOI: 10.18280/ijht.390404 [Crossref], Google Scholar

16Du, Z.; Zuo, L.; Li, J.; Liu, Y.; Shen, H. T. Data-Driven Estimation of Remaining Useful Lifetime and State of Charge for Lithium-Ion Battery. IEEE Trans. Transp. Electrif. 2022, 8, 356– 367, DOI: 10.1109/TTE.2021.3109636 [Crossref], Google Scholar

17Deng, Z. W.; Hu, X. S.; Lin, X. K.; Kim, Y.; Li, J. C. Sensitivity Analysis and Joint Estimation of Parameters and States for All-Solid-State Batteries. IEEE Trans. Transp. Electrif. 2021, 7, 1314– 1323, DOI: 10.1109/TTE.2021.3050987 [Crossref], Google Scholar

18Meng, J. H.; Stroe, D. I.; Ricco, M.; Luo, G. Z.; Swierczynski, M.; Teodorescu, R. A Novel Multiple Correction Approach for Fast Open Circuit Voltage Prediction of Lithium-Ion Battery. IEEE Trans. Energy Convers. 2019, 34, 1115– 1123, DOI: 10.1109/TEC.2018.2880561 [Crossref], Google Scholar

19Xiao, Z. Y.; Wu, S. Q. Discharge Curve-Based Formation of Retired Power Batteries for Secondary Use. Int. J. Low-Carbon Technol. 2021, 16, 790– 797, DOI: 10.1093/ijlct/ctab010 [Crossref], [CAS], Google Scholar

20Jiang, C.; Wang, S. L.; Wu, B.; Etse-Dabu, B.; Xiong, X. A Novel Adaptive Extended Kalman Filtering and Electrochemical-Circuit Combined Modeling Method for the Online Ternary Battery state-of-charge Estimation. Int. J. Electrochem. Sci. 2020, 15, 9720– 9733, DOI: 10.20964/2020.10.09 [Crossref], Google Scholar

21How, D. N. T.; Hannan, M. A.; Lipu, M. S. H.; Ker, P. J. State of Charge Estimation for Lithium-Ion Batteries Using Model-Based and Data-Driven Methods: A Review. IEEE Access 2019, 7, 136116– 136136, DOI: 10.1109/ACCESS.2019.2942213 [Crossref], Google Scholar

22Wang, W. D.; Wang, X. T.; Xiang, C. L.; Wei, C.; Zhao, Y. L. Unscented Kalman Filter-Based Battery SOC Estimation and Peak Power Prediction Method for Power Distribution of Hybrid Electric Vehicles. IEEE Access 2018, 6, 35957– 35965, DOI: 10.1109/ACCESS.2018.2850743 [Crossref], Google Scholar

23Zhang, K.; Ma, J.; Zhao, X.; Zhang, D. Y.; He, Y. L. State of Charge Estimation for Lithium Battery Based on Adaptively Weighting Cubature Particle Filter. IEEE Access 2019, 7, 166657– 166666, DOI: 10.1109/ACCESS.2019.2953478 [Crossref], Google Scholar

24Rosewater, D.; Baldick, R.; Santoso, S. Risk-Averse Model Predictive Control Design for Battery Energy Storage Systems. IEEE Trans. Smart Grid 2020, 11, 2014– 2022, DOI: 10.1109/TSG.2019.2946130 [Crossref], Google Scholar

25Li, H. H.; Wang, X. Y.; Saini, A.; Zhu, Y. Q.; Wang, Y. P. State of Charge Estimation for Lithium-Ion Battery Models Based on a Thermoelectric Coupling Model. Int. J. Electrochem. Sci. 2020, 15, 3807– 3824, DOI: 10.20964/2020.05.41 [Crossref], [CAS], Google Scholar

26Liu, T. Y.; Cheng, S. S.; Wei, Y. H.; Li, A.; Wang, Y. Fractional Central Difference Kalman Filter with Unknown Prior Information. Signal Process. 2019, 154, 294– 303, DOI: 10.1016/j.sigpro.2018.08.006 [Crossref], Google Scholar

27Loumponias, K.; Vretos, N.; Tsaklidis, G.; Daras, P. An Improved Tobit Kalman Filter with Adaptive Censoring Limits. Circuits, Syst. Signal Process. 2020, 39, 5588– 5617, DOI: 10.1007/s00034-020-01422-w [Crossref], Google Scholar

28Chi, Y. T.; Qiu, Y. W.; Lin, J.; Song, Y. H.; Li, W. Y.; Hu, Q.; Mu, S. J.; Liu, M. A Robust Surrogate Model of a Solid Oxide Cell Based on an Adaptive Polynomial Approximation Method. Int. J. Hydrogen Energy 2020, 45, 32949– 32971, DOI: 10.1016/j.ijhydene.2020.09.116 [Crossref], [CAS], Google Scholar

29Guo, N.; Fang, Y.; Tian, Z. L.; Cao, S. Y. Research on SOC Fuzzy Weighted Algorithm Based on GA-BP Neural Network and Ampere Integral Method. J. Eng. 2019, 2019, 576– 580, DOI: 10.1049/joe.2018.9385 [Crossref], Google Scholar

30Li, C.; Xiao, F.; Fan, Y.; Tang, X.; Yang, G. Joint Estimation of the State of Charge and the State of Health Based on Deep Learning for Lithium-Ion Batteries. Proc. Chin. Soc. Electr. Eng. 2021, 41, 681–691Google Scholar

31Wang, Y.; Li, J.; Zhang, F. Battery State Estimation of Least Squares Support Vector Machinebased on Particle Swarm Optimization. Energy Storage Sci. Technol. 2020, 9, 1153– 1158Google Scholar

32Li, P. Q.; Tan, Z. X.; Zhou, Y. J.; Li, C. B.; Li, R.; Qi, X. Z. Secondary Frequency Regulation Strategy With Fuzzy Logic Method and Self-Adaptive Modification of State of Charge. IEEE Access 2018, 6, 43575–43585, DOI: 10.1109/ACCESS.2018.2859354 [Crossref], Google Scholar

33Chen, Z.; Li, L.; Shu, X.; Shen, S.; Liu, Y.; Shen, J. Efficient Remaining Capacity Estimation Method for LIB Based on Feature Processing and the RBF Neural Network. Energy Storage Sci. Technol. 2021, 10, 261– 270Google Scholar

34Zhang, Z. J.; Hou, R.; Yang, J. Detection of Social Network Spam Based on Improved Extreme Learning Machine. IEEE Access 2020, 8, 112003– 112014, DOI: 10.1109/ACCESS.2020.3002940 [Crossref], Google Scholar

35Zhang, M. Y.; Wu, Q.; Xu, Z. Z. Tuning Extreme Learning Machine by an Improved Electromagnetism-Like Mechanism Algorithm for Classification Problem. Math. Biosci. Eng. 2019, 16, 4692–4707[PubMed], [CAS], Google Scholar

36Xu, R.; Liang, X.; Ma, Y.; Qi, J. Adaptive Orthogonal Search for Network Structure Learning of ELM. Chin. J. Comput. 2021, 44, 1888– 1906Google Scholar

37Wang, Q.; Wei, M.; Ye, M.; Li, J.; Xu, X. Estimation of Lithium-Ion Battery SOC Based on GWO-Optimized Extreme Learning Machine. Energy Storage Sci. Technol. 2021, 10, 744– 751Google Scholar

38Lipu, M. S. H.; Hannan, M. A.; Hussain, A.; Saad, M. H.; Ayob, A.; Uddin, M. N. Extreme Learning Machine Model for State-of-Charge Estimation of Lithium-Ion Battery Using Gravitational Search Algorithm. IEEE Trans. Ind. Appl. 2019, 55, 4225– 4234, DOI: 10.1109/TIA.2019.2902532 [Crossref], Google Scholar

39Emami, S. A.; Ahmadi, K. K. A. A Self-Organizing Multi-Model Ensemble for Identification of Nonlinear Time-Varying Dynamics of Aerial Vehicles. Proc. Inst. Mech. Eng., Part I 2021, 235, 1164–1178, DOI: 10.1177/0959651820975245 [Crossref], Google Scholar

40He, C. M.; Liu, Y. Q.; Yao, T.; Xu, F. H.; Hu, Y. Y.; Zheng, J. H. A Fast Learning Algorithm Based on Extreme Learning Machine for Regular Fuzzy Neural Network. J. Intell. Fuzzy Syst. 2019, 36, 3263–3269, DOI: 10.3233/jifs-18046 [Crossref], Google Scholar

41Liu, Y. L.; Wang, J. Y.; Yue, Z. Y. Improved Multi-Point Estimation Method Based Probabilistic Transient Stability Assessment for Power System with Wind Power. Int. J. Electr. Power Energy Systems 2022, 142, 108283 DOI: 10.1016/j.ijepes.2022.108283 [Crossref], Google Scholar

42Tan, Z. G.; Xiao, L.; Chen, S. Y.; Lv, X. J. Noise-Tolerant and Finite-Time Convergent ZNN Models for Dynamic Matrix Moore-Penrose Inversion. IEEE Trans. Ind. Inf. 2020, 16, 1591– 1601, DOI: 10.1109/TII.2019.2929055 [Crossref], Google Scholar

43Ren, X. Q.; Liu, S. L.; Yu, X. D.; Dong, X. A Method for State-of-Charge Estimation of Lithium-Ion Batteries Based on PSO-LSTM. Energy 2021, 234, 121236 DOI: 10.1016/j.energy.2021.121236 [Crossref], Google Scholar

44Gopalakrishnan, S. K.; Kinattingal, S.; Simon, S. P. MPPT in PV Systems Using PSO Appended with Centripetal Instinct Attribute. Electr. Power Compon. Systems 2020, 48, 881– 891, DOI: 10.1080/15325008.2020.1825552 [Crossref], Google Scholar

45Huang, Q. H.; Wang, X. A Forecasting Model of Wind Power Based on IPSO-LSTM and Classified Fusion. Energies 2022, 15, 5531 DOI: 10.3390/en15155531 [Crossref], Google Scholar

46Chen, Y. J.; Chen, Z. S. A Prediction Model of Wall Shear Stress for Ultra-High-Pressure Water-Jet Nozzle Based on Hybrid BP Neural Network. Eng. Appl. Comput. Fluid Mech. 2022, 16, 1902– 1920, DOI: 10.1080/19942060.2022.2123404 [Crossref], Google Scholar

47Naidji, M.; Boudour, M. Stochastic Multi-Objective Optimal Reactive Power Dispatch Considering Load and Renewable Energy Sources Uncertainties: a Case Study of the Adrar Isolated Power System. Int.Trans. Electr. Energy Systems 2020, 30, e12374 DOI: 10.1002/2050-7038.12374 [Crossref], Google Scholar

48Ren, M. L.; Huang, X. D.; Zhu, X. X.; Shao, L. J. Optimized PSO Algorithm Based on the Simplicial Algorithm of Fixed Point Theory. Appl. Intell. 2020, 50, 2009– 2024, DOI: 10.1007/s10489-020-01630-6 [Crossref], Google Scholar

49Chin, C. S.; Gao, Z. C. State-of-Charge Estimation of Battery Pack under Varying Ambient Temperature Using an Adaptive Sequential Extreme Learning Machine. Energies 2018, 11, 711 DOI: 10.3390/en11040711 [Crossref], Google Scholar

50Zhu, J.; Tan, T. X.; Wu, L. F.; Yuan, H. M. RUL Prediction of Lithium-Ion Battery Based on Improved DGWO-ELM Method in a Random Discharge Rates Environment. IEEE Access 2019, 7, 125176– 125187, DOI: 10.1109/ACCESS.2019.2936822 [Crossref], Google Scholar